1.0
1.1
1.25
1.4
1.6
1.8
2.0
2.2
2.5
2.8
3.2
3.6
4.0
4.5
5.0
5.6

1 of 1

GA–A21554

RECENT VH–MODE RESULTS ON DIII–D

by

T.H. OSBORNE, K.H. BURRELL, T.N. CARLSTROM, M.S. CHU, J.C. DeBOO, E.J. DOYLE,*
J.R. FERRON, P. GOHIL, C.M. GREENFIELD, R.J. GROEBNER, A.W. HYATT, G.L. JACKSON,
Y.B. KIM, S. KONOSHIMA,† T.K. KURKI-SUONIO,‡ R.J. LA HAYE, E.A. LAZARUS,♯ L.L. LAO,
S.I. LIPPMANN, T.W. PETRIE, C.L. RETTIG,* R.D. STAMBAUGH, G.M. STAEBLER,
H. St. JOHN, E.J. STRAIT, T.S. TAYLOR, S.J. THOMPSON, A.D. TURNBULL,
D. WRÓBLEWSKI,♭ and The DIII–D TEAM

This is a preprint of a paper to be presented at the Fourth H–Mode Workshop, November 15–17, 1993, Naka, Japan, and to be printed in *Plasma Physics and Controlled Fusion.*

Work supported by
U.S. Department of Energy
Contract Nos. DE-AC03-89ER51114,
DE-FG03-86ER53225, W-7405-ENG-48,
and DE-AC05-84OR21400.

* University of California at Los Angeles.
† Japan Atomic Energy Research Institute.
‡ Helsinki University of Technology.
♯ Oak Ridge National Laboratory.
♭ Lawrence Livermore National Laboratory.

GENERAL ATOMICS PROJECT 3466
JANUARY 1994

GENERAL ATOMICS

Recent VH–Mode Results on DIII–D*

T.H. OSBORNE, K.H. BURRELL, T.N. CARLSTROM, M.S. CHU, J.C. DEBOO, E.J. DOYLE,[a] J.R. FERRON, P. GOHIL, C.M. GREENFIELD, R.J. GROEBNER, A.W. HYATT, G.L. JACKSON, Y.B. KIM, S. KONOSHIMA,[b] T.K. KURKI-SUONIO,[c] R.J. LA HAYE, E.A. LAZARUS,[d] L.L. LAO, S.I. LIPPMANN, T.W. PETRIE, C.L. RETTIG,[a] R.D. STAMBAUGH, G.M. STAEBLER, H. ST. JOHN, E.J. STRAIT, T.S. TAYLOR, S.J. THOMPSON, A.D. TURNBULL, D. WRÓBLEWSKI,[e] AND THE DIII–D TEAM

General Atomics, P.O. Box 85608, San Diego, California 92186-9784, U.S.A.

(Received

Abstract. A regime of improved H–mode energy confinement, VH–mode, is obtained in the DIII–D tokamak with adequate vessel conditioning. The improved confinement in VH–mode is consistent with the extension of the region of high $E \times B$ velocity shear turbulence suppression zone further in from the plasma boundary. The energy confinement enhancement in VH–mode can be limited by ELMs, localized momentum transfer events, or operation at high heating power or low q. Energy confinement enhancement improves with increasing triangularity of the plasma cross section and is independent of elongation. The termination of VH–mode is associated with an edge localized kink mode which is destabilized by both the large edge pressure gradient and edge current density.

1. Introduction

Very high (VH)–mode (JACKSON *et al.* 1991) is a regime of improved H–mode confinement relative to an energy confinement time scaling derived from fitting pre-1990 DIII–D and JET ELM-free thermal energy confinement. JET/DIII–D scaling (SCHISSEL *et al.* 1991) $\tau_E^{JET/DIII-D} = 0.106\, I_P^{1.03}\,(\mathrm{MA}) R^{1.48}\,(\mathrm{m}) P_{LOSS}^{-0.46}\,(\mathrm{MW})$, where $P_{LOSS} = P_{Heating} - dW_{Total}/dt$, also is consistent with the ASDEX data. VH–mode exceeds this scaling by a factor of approximately 2 for both JET and DIII–D (GREENFIELD *et al.* 1993).

There were several improvements in VH–mode performance in 1993. Prior to 1993 it was necessary to condition the DIII–D vacuum vessel with boronization to produce VH–mode (JACKSON *et al.* 1991). In 1993, after the installation of graphite armor on the outboard vessel wall giving full graphite coverage, we also produced VH–mode discharges. The graphite tiles were conditioned by baking and glow discharge cleaning in helium. The well conditioned full graphite wall produced discharges with lower radiated power, lower high Z and similar low Z impurities, and similar low recycling to the boronized case. In 1993 we also produced VH–mode discharges with $\tau_N = \tau_E^{TH}/\tau_{JET/DIII-D} \approx 2.2$, $H = \tau_E^{DIA}/\tau_{ITER-89P} \approx 3.8$, $\beta_N = \beta_T/(I/aB) \approx 4$, $\beta_N \tau_N = 7.3$ compared to 6.0 in 1992 by improving the β limit at high τ_N with a plasma current ramp down, $\beta_T \tau_E \approx 1.6$%-s was produced compared to 1.3 in 1992 with discharges at high plasma current, and $n_D(0) T_i(0) \tau_E^{TH} \approx 4 \times 10^{20}\,\mathrm{m}^{-3}\,\mathrm{keV\text{-}s}$ (2×10^{20} was obtained in 1992), in a hot ion VH–mode.

In this paper we first describe the $E \times B$ velocity shear penetration hypothesis for the confinement enhancement in VH–mode. We then describe some of the effects which interact to set the peak τ_N achieved in VH–mode, and finally the VH–mode terminating event.

* Work supported by the U.S. Department of Energy under Contract Nos. DE-AC03-89ER51114, DE-FG03-86ER53225, W-7405-ENG-48, and DE-AC05-84OR21400.

a) University of California at Los Angeles.

b) Japan Atomic Energy Research Institute.

c) Helsinki University of Technology.

d) Oak Ridge National Laboratories.

e) Lawrence Livermore National Laboratory.

2. $E \times B$ velocity shear and VH–mode

The formation of a transport barrier near the plasma boundary, by the $E_r \times B$ velocity shear suppression of turbulence, is a leading candidate for the cause of confinement improvement in H–mode (GROEBNER *et al.* 1993). In VH–mode, the $E \times B$ velocity shear penetrates further in from the plasma edge, which may result in a larger turbulence suppression and improved confinement region.

The region where the the $E \times B$ velocity shear increases in VH–mode corresponds to the region of greatest improvement in energy confinement. Fig. 1 shows the change in the profiles of E_r, $E \times B$ velocity shear, and effective thermal diffusivity, $\chi_{\rm eff}$, during a VH–mode discharge. E_r changes from a broad profile, with high shear only near the plasma boundary, to a profile peaked near $\rho = 0.5$, which results in a penetration of the $E \times B$ velocity shear. The $E \times B$ velocity shear is increased in the region where the greatest reduction in $\chi_{\rm eff}$ is computed. E_r is determined using the CER diagnostic (GOHIL *et al.* 1990) measurement of impurity pressure gradient and poloidal and toroidal rotation speed through the lowest order radial force balance, $E_r = -\mathbf{v_I} \times \mathbf{B} + 1/(n_I Z_I e)\nabla P_I$ (HINTON 1976), and $V'_{E\times B} \equiv (B/B_T)d(E_r/B)/dR$ where B is the total field. The effective single fluid thermal diffusivity, $\chi_{\rm eff} = -(q_e + q_i)/(n_e \nabla T_e + n_e \nabla T_e)$, where q_e and q_i are respectively the electron and ion heat flux. The transport analysis was carried out using the ONETWO transport code (PFEIFFER *et al.* 1985). The profiles in Fig. 1 are for the outboard midplane. The $E \times B$ velocity shear is found to be of significant magnitude for turbulence suppression when compared to the Biglari, Diamond, Terry (BIGLARI 1990) expression using fluctuation measurements in the H–mode pedestal region (DOYLE *et al.* 1992), as well as when compared to the Hassam estimate of C_s/R (HASSAM 1991) as shown in Fig. 1.

The temporal evolution of the $E \times B$ velocity shear penetration follows the development of the confinement enhancement in VH–mode (Fig. 2) where the penetration depth of significant $E \times B$ velocity shear is defined as the radial location at which the Biglari-Diamond-Terry (BDT) criteria is met.

Using an externally applied $n = 1$ error field we were able to reduce the $E \times B$ velocity shear and subsequently the energy confinement enhancement in VH–mode (LA HAYE *et al.* 1993) (Fig. 3). Since the externally applied error field only acts as a localized drag or momentum sink, this experiment suggests

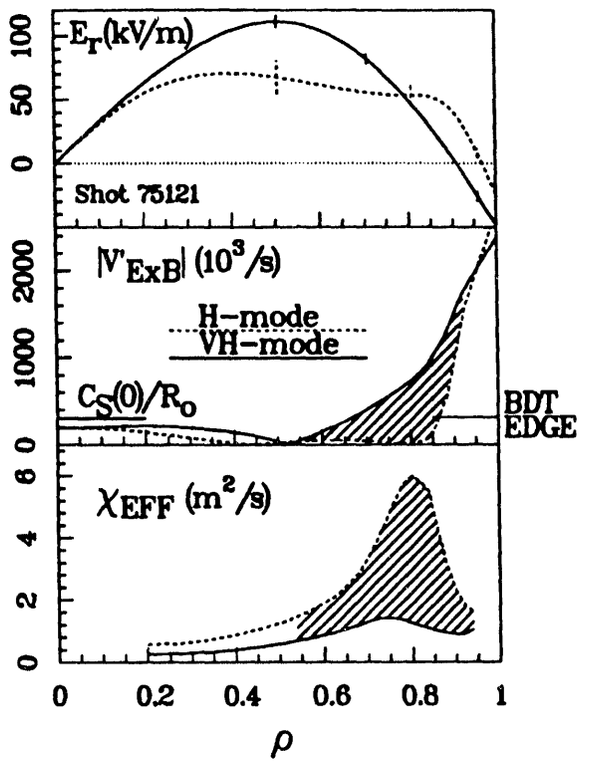

Figure 1. Comparison of H–mode (dash) and VH–mode radial electric field, E_r; $E \times B$ velocity shear, $V'_{E\times B}$; and effective thermal diffusivity, $\chi_{\rm eff}$; vs. normalized radial coordinate, ρ. Also shown are the BDT and C_s/R velocity shear estimates required for turbulence suppression.

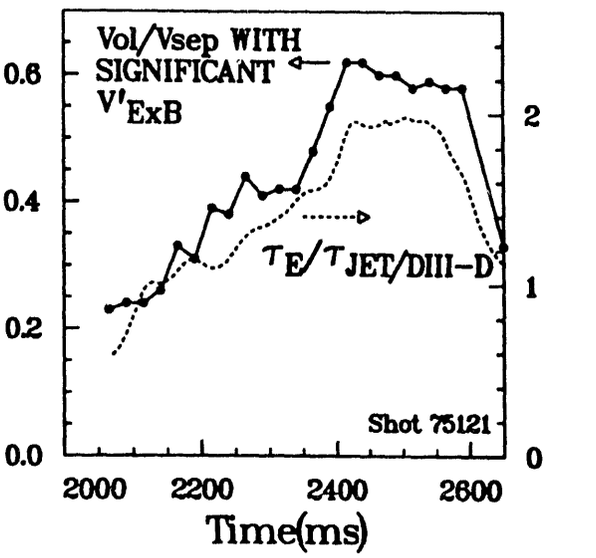

Figure 2. Time history of τ_N (dash); and a measure of the fractional volume inside the separatrix with sufficient $E \times B$ velocity shear for turbulence suppression (BDT estimate).

that the enlarged region of the $E \times B$ velocity shear is the cause of the improved confinement in VH–mode rather than the result of the steepening of the rotation and pressure gradients. We believe that the magnetic islands generated by the $n = 1$ error field have a negligible direct effect on energy confinement since no change in τ_E is observed when the error field is applied to an L–mode discharge.

3. Factors which affect the peak τ_N

The variation of peak τ_N in double-null divertor discharges as a function of discharge shape, q_{95} (safety factor at 95% of the poloidal flux between the magnetic axis and separatrix), and input heating power are shown in Fig. 4. The highest τ_N is obtained in high triangularity discharges, with little variation in τ_N with elongation between 1.7 and 2. For a given shape τ_N peaks at moderate q (between 4 and 6), and degrades at high input power and in some cases at low power as well.

One factor which controls the maximum confinement obtained in a VH–mode discharge is the duration of the edge localized mode (ELM)-free period. τ_N rises on an energy transport time scale in VH–mode. As shown in Fig. 5, τ_N is either clamped or reduced when ELMs begin. The effect of ELMs may be to limit the penetration of the $E \times B$ velocity shear. The variation of ELM-free period with power can be complex as is illustrated in Fig. 6. Beginning at low power, the ELM-free period at first decreases with power until a critical power is reached at which it increases markedly, followed by another decrease. Above this critical power the first ELM has the characteristics of the terminating event described in Sec. 4. The rate of rise of τ_N increases with increasing power. From the product of these two curves τ_N is expected to be limited by ELMs below the critical power. This was responsible for the power threshold for VH–mode observed in 1991 for the $\kappa = 2$, $\delta = 0.9$ double-null divertor discharges, and is responsible for the degradation in τ_N at low power observed in 1993 $\kappa = 1.7$, $\delta = 0.9$ discharges. In 1992 and 1993 the $\kappa = 2$, $\delta = 0.9$ double-null discharges it was possible to extend the high power branch of the ELM-free period down to 5 MW, and τ_N now peaks at low power as shown in Fig. 4. High plasma density or recycling prevents access to the regime of long ELM-free period at high heating power. The two discharges of Fig. 5 differ only in that the discharge with short ELM-free period had about 30% shorter duration He glow conditioning between shots.

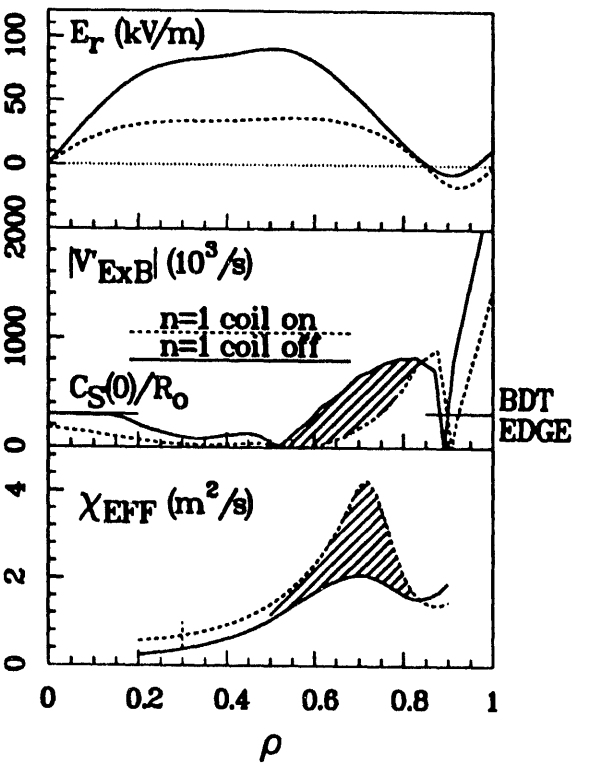

Figure 3. Comparison of discharges with (dash) and without magnetic braking. Quantities defined as in Fig. 2. Magnetic braking reduces $V'_{E\times B}$ and increases χ_{eff}.

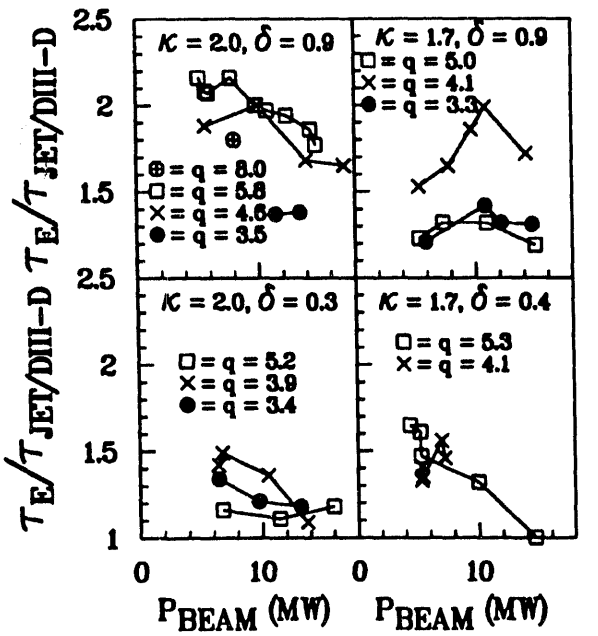

Figure 4. Effect of plasma shape, q_{95}, and input heating power on τ_N for double-null divertor discharges.

The degradation of confinement enhancement at high power is illustrated in Fig. 7. Although initially τ_N rises more rapidly in the higher power case, it saturates at a lower level. This saturation is associated with a degradation in the velocity shear and rise in density fluctuations, and is not connected with the reduction in ELM-free period at high power. The β_N value at which the fluctuations rise and τ_N saturates increases with input power suggesting the degradation is not β related. Also there are no low n MHD modes consistently observed at the confinement degradation.

A similar degradation in confinement and associated reduction in velocity shear is observed during the ELM-free period of low q discharges. This degradation is not associated with ELMs or sawteeth. It is unclear at present whether the reduction in τ_N at high input power and low q are related phenomena.

Another phenomenon which controls the confinement enhancement in VH–mode are density fluctuation bursts observed on the far infrared scattering diagnostic, FIR (RETTIG *et al.* 1990) which are associated with localized momentum transport events MTEs. Fig. 8 illustrates this phenomenon and its effect on rotational shear for the discharge of Fig. 2. A rapid increase in the $E \times B$ velocity shear penetration and in τ_N can be seen near the time of the cessation of the MTEs in Fig. 2. At each MTE there is a drop in rotation near $\rho = 0.6$ and rise near $\rho = 0.8$ which can be seen in the isolated event near 2.5 s in Fig. 8. The density fluctuations during an MTE peat at 1 MHz for $\kappa_\theta = 2$ cm^{-1} and extend ± 500 kHz from this peak. No low n MHD modes are associated with MTEs. Small ELM-like spikes are sometimes seen on the divertor D_α emission at an MTE. ELMs however have a SXR inversion at the separatrix while MTE show an inversion 5 to 10 cm inside the separatrix. The frequency distribution of the density fluctuations at an MTE, if interpreted as doppler shift, indicate that the fluctuations are coming from approximately the same region of the plasma where the momentum transfer is occuring. The high frequency MTEs before 2.35 s in Fig. 8 are thus thought to produce the observed flat spot in the toroidal rotation profile roughly between ρ=0.6 and 0.8 resulting in high $E \times B$ velocity shear only outside $\rho = 0.8$. Discharges in which MTEs are continuous and high frequency for the duration of the ELM-free period do not exceed τ_N of 1.5. The time between the L-H transition and the rapid increase in the velocity shear at the cessation of

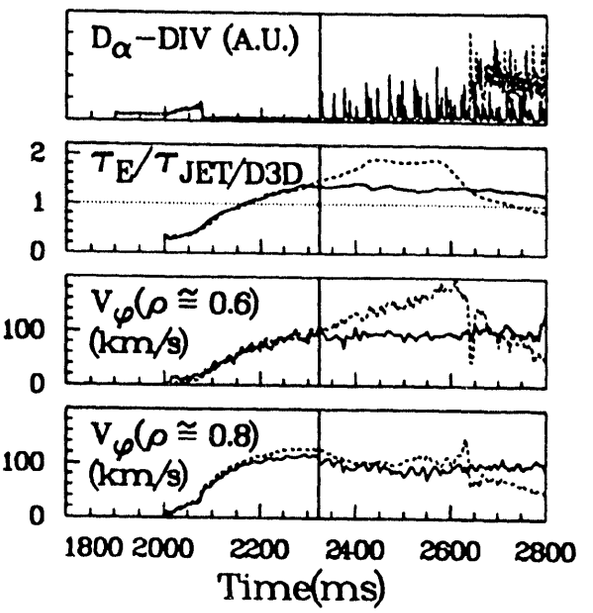

Figure 5. Effect of ELMs on VH–mode. τ_N is clamped at early ELM onset. Rotational shear does not penetrate with ELMs.

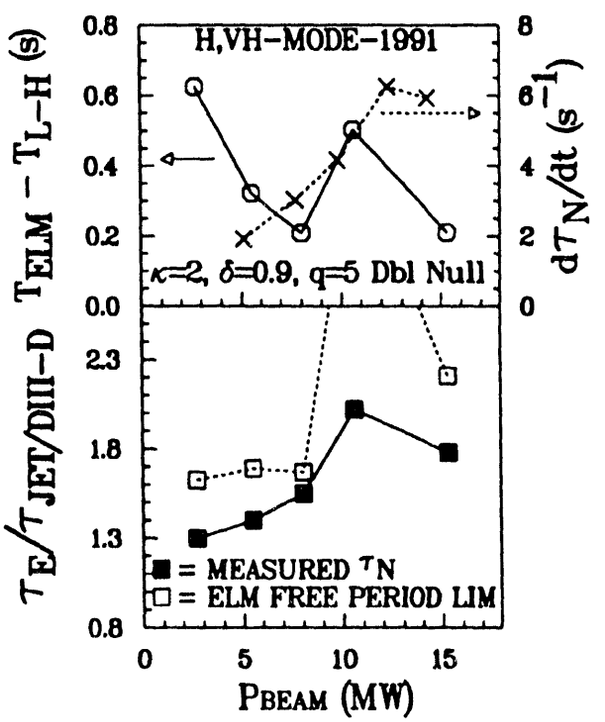

Figure 6. Variation with NBI power of the duration of the ELM-free period (solid), the rate of rise of τ_N (dash); the achieved τ_N (solid); and the τ_N which would be expected if it was limited by the duration of the ELM-free period. Data from 1991 boronized double-null divertor discharges.

the MTEs, which we call the spin-up time, decreases with increasing input power and with decreasing q_{95}. The MTEs effect appears to be responsible for the confinement degradation at low triangularity when discharges limited by other effects are excluded.

The interaction of the rate of rise of τ_N with the duration of the ELM-free period, the time to spin-up, and the degradation at high power and low q is responsible for the τ_N variation shown in Fig. 4.

4. VH–Mode termination

The ELM-free phase of a VH–mode discharge is often terminated by a global energy loss, followed by rapid ELMs and a large reduction in τ_E. The event is initiated by a medium n mode rotating in the electron diamagnetic drift direction which grows on a time scale of 20 to 50 μs. In addition to the fact that rotation in the electron drift direction is consistent with the negative electric field at the plasma edge, soft x-ray measurements also suggest that this mode is edge localized. In addition to this rapidly growing mode, low n modes ($n = 1$ or 2) rotating in the ion drift direction, which corresponds to the direction of NBI, are observed growing on a time scale of 10s of milliseconds before the termination. Using experimentally determined equilibria, ideal kink stability calculations, using the GATO code (BERNARD *et al.* 1981), show ideal edge localized modes with $n = 2, 3, 4$ to be unstable just before the termination, while these modes are stable shortly after the L to H transition. Both the edge current, which grows continuously in VH–mode probably due to bootstrap current associated with the large edge pressure pedestal, and the edge pressure gradient are destabilizing to this mode. By employing a current ramp down in VH–mode we were able to reduce the edge current density and increase the β limit. This technique resulted in the highest $\beta_N \tau_N$ of 7.3 achieved on DIII–D.

5. Discussion

The data strongly suggest that $E \times B$ velocity shear is important in the confinement improvement in VH–mode. Other factors may also be important. There is a small increase in the internal inductance ℓ_i during VH–mode. Based on current ramp down data for L–mode discharges (ZARNSTROFF *et al.* 1990) this ℓ_i change is too small to account for the confinement improvement in VH–mode. Experiments in which both the magnetic and $E \times B$ velocity shear are increased (LAO *et al.* 1993)

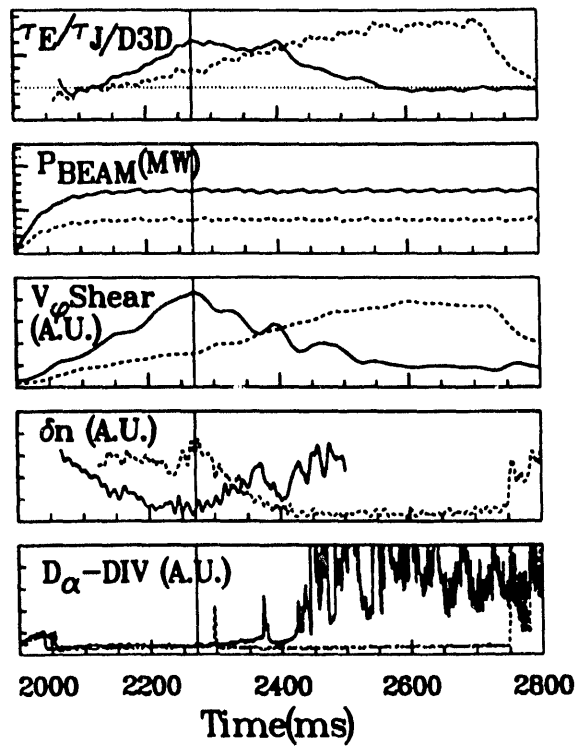

Figure 7. τ_N is reduced at high input power. τ_N saturates when velocity shear is reduced and density fluctuations increase. The time of τ_N saturation velocity shear reduction and density fluctuation increase in the higher power discharge is marked.

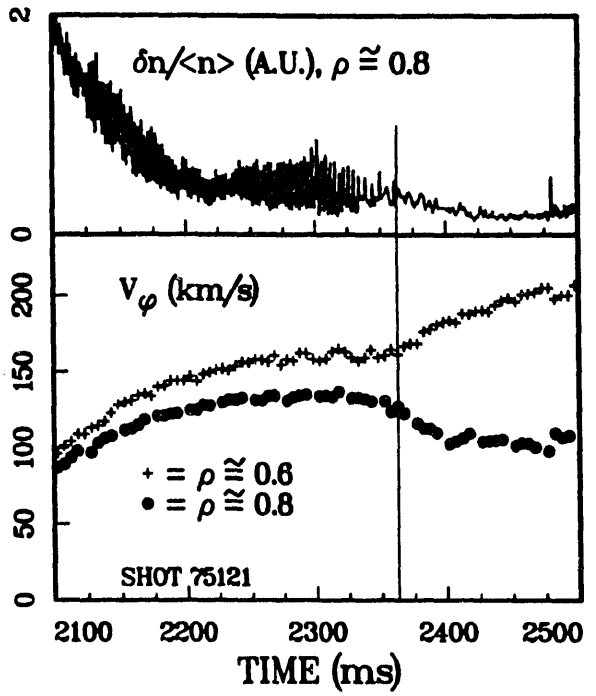

Figure 8. Velocity shear increases when fluctuation bursts, MTEs, from approximately the same region of the plasma cease. The time of MTE cessaton and velocity shear increase is marked.

indicate the effect may be additive, suggesting they may operate on different loss channels. The connection between E_r and the rotation speeds and pressure gradient through the radial force balance suggests a positive feedback mechanism may exist whereby an increase in rotational shear or pressure gradient produces an increase in $E \times B$ velocity shear, reducing transport through turbulence suppression and allowing a further increase in rotational shear and pressure gradient. This picture is explored in detail in the theoretical work of Hinton and Staebler (1993) and is consistent with the gradual penetration of $E \times B$ velocity shear and confinement improvement and with the importance of low impurity radiation.

The two regimes of ELM-free period at low and high power shown in Fig. 6 may be the result of second stability to ballooning modes in the plasma edge at high power. The character of the first ELM is different in the two regimes. At high power the first ELM is the terminating event described above, at low power the first ELM is edge localized and is not accompanied by the fast growing medium n mode. Double-null divertor discharges at $\kappa = 2$, $\delta = 0.9$, and $q = 5$ are found to have access to the second stable regime for ideal ballooning modes throughout the ELM-free period. The reason why input power or plasma wall conditions (Fig. 5) would effect edge second stability is unclear, possibly resistive ballooning modes which have a lower pressure gradient threshold become important at low power or high density. Plasma shape also appears to play a role. The confinement enhancement at low triangularity was limited by the fact that long ELM-free periods at high input power could not be achieved even with improved wall conditions. The reason for confinement degradation at high power and low q is not clear. Although ballooning stability is not obviously implicated a more detailed study of the stability of these plasmas is needed.

On JET, τ_N values of $\approx$2 are obtained at triangularity of 0.4 (GREENFIELD *et al.* 1993), while on DIII–D, τ_N values at this low triangularity were typically 1.5. MTEs have not been observed on JET. The difference in the results on the two devices may represent differences in the parametric variation of the controlling processes. For example on JET it was possible to obtain long ELM-free periods at high power following an ELMing phase when the edge became second stable. This type of behavior was not observed in the low triangularity double-null discharges on DIII–D but was obtained with JET like shape and discharge preparation.

The global nature of the terminating event is not understood since the associated mode is edge localized. A coupling of the medium n edge mode with the internal low n modes may be responsible for the global nature of the termination.

When ELMs, MTEs and the problems of low q and high power are avoided the energy confinement saturates at about 2 times $\tau_{JET/DIII-D}$. A similar maximum value is obtained in both JET and DIII–D. It is unclear whether this represents a limit on the confinement enhancement in VH–mode. Improvement in the VH–mode confinement enhancement is an exciting prospect for future work.

References

Bernard, L.C., *et al.* (1981). *Comput. Phys. Commum.* **24**, 377.

Biglari, H. (1990). *Phys. Fluids B* **2** 1.

Doyle, E.J., *et al.* (1992). *Plasma Phys. and Controlled Nucl. Fusion Research 1992*, (IAEA, Vienna) Vol. 1, p. 235.

Greenfield, G.C., *et al.* (1993). JET report JET-P(93)75, to be published in *Plasma Phys. and Contr. Fusion* December 1993.

Gohil, P., *et al.* (1990). *Rev. Sci. Instrum.*, **61**, 2949.

Groebner, R.J., *et al.* (1993). *Phys. Fluids B*, **5**, 2343.

Hassam, A.B. (1991). *Comments on Plasma Phys. and Contr. Fusion* **14**, 275.

Hinton, F.L. and R.D. Hazeltine (1976). *Rev. Mod. Phys.* **48**, 239.

Jackson, G.L. *et al.* (1991). *Phys. Rev. Lett.* **67**, 3098.

La Haye, R.J., *et al.* (1993). General Atomics Rep. GA-A21544, submitted to *Phys. Rev. Lett.*

Lao, L.L., *et al.* (1993). *Phys. Rev. Lett.* **70**, 3435.

Pfeiffer, W., *et al.* (1985). *Nucl. Fusion* **25**, 655.

Rettig, C.L., S. Burns, R. Philipona, *et al.* (1990). *Rev. Sci. Instrum.* **61**, 3010.

Schissel, D.P., *et al.* (1991). *Nucl. Fusion* **31**, 73.

Staebler, G.M., *et al.* (1993). General Atomics Rep. GA-A21278, submitted to *Phys. Plasmas.*

Zarnstroff, M.C., *et al.* (1991). *Plasma Phys. and Contr. Nucl. Fusion Research, 1990* (IAEA, Vienna, 1991), Vol. 1, p. 109.

DATE FILMED

4/7/94

END